Available online at www.sciencedirect.com
SCIENCE DIRECT®
Aerospace Science and Technology 9 (2005) 261–271
Aerospace Science and Technology
www.elsevier.com/locate/aescte

Reduced dynamic orbit determination using GPS code and carrier measurements

Reduziert-dynamische Bahnbestimmung mit GPS Code- und Phasenmessungen

Oliver Montenbruck [a,*], Tom van Helleputte [b], Remco Kroes [b], Eberhard Gill [a]

[a] *German Space Operations Center, Deutsches Zentrum für Luft- und Raumfahrt, 82230 Weßling, Germany*
[b] *Department of Earth Observation and Space Systems, Delft University of Technology, 2629 HS Delft, The Netherlands*

Received 28 October 2004; received in revised form 31 December 2004; accepted 11 January 2005

Available online 25 February 2005

Abstract

The three-dimensional nature of Global Positioning System (GPS) measurements provides a unique opportunity for accurately determining the position and velocity of satellites in low Earth orbit (LEO). For optimum results a reduced dynamic technique is commonly preferred, which combines the merits of kinematic positioning techniques with those of a fully dynamic trajectory modeling. As part of the present study two different approaches to reduced dynamic orbit determination are compared, both of which involve the estimation of empirical accelerations on top of a precise deterministic force model. In the batch least-squares estimator piece-wise constant accelerations are adjusted in consecutive sub-intervals that are sufficiently short compared to the orbital period. The extended Kalman filter/smoother approach, on the other hand, estimates the empirical accelerations using a first-order Gauss–Markov process noise model. Software implementations of both estimation methods have been used with GPS measurements of the GRACE mission to assess the individual merits of the different filtering schemes. Both approaches are shown to provide accurate and compatible results, which match an external reference solution to better than 5 cm when processing dual-frequency data and better than 10 cm when using single-frequency measurements. While the extended Kalman filter/smoother requires less computer resources in terms of memory and processing time, the batch least-squares estimator ensures a better smoothness of the resulting trajectory and was found to be more robust in case of data gaps.

Zusammenfassung

Die drei-dimensionale Natur von Messungen des Global Positioning System (GPS) schafft eine ideale Voraussetzungen zur genauen Bestimmung der Position und Geschwindigkeit eines Raumfahrzeuges im niedrigen Erdorbit (LEO). Beste Ergebnisse lassen sich dabei mit reduziert-dynamischen Verfahren erzielen, die die Vorteile einer kinematischen Positionierung mit denen einer streng-dynamischen Bahnmodellierung verbinden. Im Rahmen der vorliegenden Studie werden zwei verschiedene Ansätze zur reduziert-dynamischen Bahnbestimmung verglichen, die beide auf der Schätzung empirischer Beschleunigungen in Kombination mit einem präzisen Kräftemodell basieren. Bei Ausgleichung nach der Methode der kleinsten Quadrate werden abschnittsweise konstante Beschleunigungen in Intervallen geschätzt, die ausreichend klein gegenüber der Bahnperiode sind. Beim "Extended Kalman-Filter/Smoother" werden die Beschleunigungen direkt unter Annahme eines Gauss–Markov-Prozesses erster Ordnung geschätzt. Implementierungen beider Verfahren wurden zur Prozessierung von GPS-Daten der GRACE Mission eingesetzt, um die jeweiligen Vorteile zu bewerten. Beide Ansätze liefern genaue und kompatible Ergebnisse, die mit externen Referenzlösungen bei Nutzung von Zweifrequenzmessungen auf besser als 5 cm und bei Einfrequenzmessungen auf besser als 10 cm übereinstimmen. Während der "Extended Kalman-Filter/Smoother" geringere Speicher-Resourcen und Rechenzeit

* Corresponding author. Tel.: +49 (8153) 28-1195; fax: +49 (8153) 28-1450.
E-mail address: oliver.montenbruck@dlr.de (O. Montenbruck).

1270-9638/$ – see front matter
doi:10.1016/j.ast.2005.01.003

benötigt, stellt die Ausgleichung nach der Methode der kleinsten Quadrate eine glatte Lösung sicher und erweist sich im Fall von Datenlücken als robuster.

Keywords: Orbit determination; GPS; LEO satellites; GRACE

Schlüsselwörter: Bahnbestimmung; GPS; LEO Satelliten; GRACE

1. Introduction

Over the past decade, Global Positioning System (GPS) sensors have gradually evolved into well-accepted standard tools for spacecraft navigation. Aside from onboard applications like real-time positioning or time-synchronization, GPS receivers are nowadays considered as primary tracking system for precision orbit determination in many satellite missions. Here, the accuracy, global coverage and three-dimensional nature of GPS measurements makes GPS highly competitive to other tracking systems such as Satellite Laser Ranging and DORIS.

In accord with geodetic applications, dual-frequency receivers are preferable for precise orbit determination of spacecraft in low Earth orbit (LEO) in order to eliminate ionospheric path delays and to make best use of high-accuracy carrier-phase measurements. Driven by the need of various scientific missions, a growing number of suitable receivers is being made available for space applications. Aside from JPL's BlackJack receiver [21], which is already flown on CHAMP [12], GRACE, IceSat and Jason, the European Lagrange receiver [14] and the GRAS instrument [25] are currently prepared for use on Radarsat-2, GOCE and METOP. Furthermore, the validation of commercial-off-the-shelf receivers (NovAtel OEM4-G2L) is in progress for use onboard the Canadian CASSIOPE mission [13]. To fully utilize the measurement accuracy offered by these systems adequate processing techniques are required.

Similar to terrestrial applications, the availability of multiple GPS measurements at each epoch allows the use of purely kinematic methods for spacecraft positioning (see e.g. [2,18]). Kinematic positioning requires no a priori knowledge of the spacecraft motion and can thus be applied to a wide range of mission scenarios. However, kinematic methods are particularly sensitive to erroneous measurements, unfavorable viewing geometry and outages, which notably restricts their value in practice. Dynamic orbit determination, in contrast, makes use of known physical models of the spacecraft motion to constrain the resulting position estimates. This allows an averaging of measurements from different epochs and the trajectory can even be propagated across data gaps.

On the other hand, the dynamics of real-world spacecraft in a low Earth orbit is hardly known to a level that matches the accuracy of GPS code and carrier-phase measurements. Aerodynamic forces, in particular, are not well predictable at altitudes of 300–600 km due to limitations of upper atmosphere density models and the complicated interaction of neutral gases and charged particles with the spacecraft surface. As a remedy, the concept of reduced dynamic orbit determination has been proposed [29,30]. Here, the deterministic model of the spacecraft dynamics is complemented by empirical accelerations that are adjusted along with other parameters in the orbit determination process. In this way, the available accuracy of GPS measurements may be fully exploited without sacrificing the robustness offered by dynamical orbit determination techniques.

The present study describes two different concepts for handling empirical accelerations in combination with a least-squares estimator and an extended Kalman filter. These methods are subsequently applied to GPS measurements collected onboard the GRACE satellite to assess the merits and disadvantages of each approach. Considering the absence of Selective Availability in all present and future radio navigation signals, the use of undifferenced GPS measurements in combination with known GPS clock and ephemeris products is assumed in both processing schemes.

2. Reduced dynamic orbit determination

This section provides an overview of the relevant dynamical and measurement models for GPS based satellite orbit determination. They match the implementation of the *G*PS *H*igh precision *O*rbit determination *S*oftware *T*ools (GHOST [28]) that have been employed in the subsequent GRACE data analysis. A summary of the adopted dynamical models and reference frame transformations is given in Table 1.

2.1. GPS observation model

The elementary data types provided by a GPS receiver comprise code and carrier-phase measurements that are obtained by synchronizing the incoming signal with a receiver generated replica [17]. The code phase (or pseudo-range) ρ_{PR} can be modeled as the sum of the true distance $|\boldsymbol{r} - \boldsymbol{r}_{\mathrm{GPS}}|$ and a term $c \cdot (\delta t - \delta t_{\mathrm{GPS}})$ which describes the difference of the receiver and satellite clock offsets. While the GPS satellite clock offset can be assumed to be known with adequate accuracy from pre-computed GPS ephemeris and clock products [11], the receiver clock offset $c\delta t$ is essentially unknown and has to be determined at each epoch as part of the orbit determination process. GPS carrier-phase measurements offer a notably lower noise (1 mm versus 0.1–1 m) than code measurements, but exhibit an unknown

bias B that must be estimated along with other parameters (e.g. state vector, clock offset, etc.).

For dual-frequency receivers, ionosphere-free linear combinations of the code and carrier-phase measurements can be formed, which make use of the fact that the ionospheric path delay is essentially proportional to the inverse square of the signal frequency. For single-frequency observations the ionospheric contribution cannot be individually eliminated from the code and carrier-phase but an ionosphere-free biased pseudo-range can be obtained from the arithmetic mean of the C/A code and L1 carrier-phase measurement [31]. This so-called GRAPHIC (*Gr*oup *A*nd *Ph*ase *I*onospheric *C*orrection) measurement can be processed similar to ionosphere-free carrier-phases even though it exhibits a notably larger noise level. In both cases an unknown bias has to be estimated as part of the orbit determination process. This bias is different for each observed GPS satellite but constant between epochs during uninterrupted carrier-phase tracking.

Within the orbit determination process, modeled observations are computed based on known GPS satellite positions and clock offsets. Using precise ephemeris products provided by the International GPS Service (IGS) [6] or its individual analysis centers, the root-mean-square (rms) GPS position error is presently on the order of five centimeters. Using an 8th order Lagrange interpolation, intermediate positions of similar accuracy can be obtained from 15 min grid points. Clock data, on the other hand, cannot be properly interpolated by high order polynomials and require smaller intervals along with linear interpolation [J. Kouba, priv. comm.]. Comparisons performed by the authors have shown that 5 min clock products can reduce the range modeling error from roughly 8 cm to 3 cm in accord with clock interpolation errors reported in [32]. A further reduction to 1 cm or better is achieved by use of 30 s clock products, which are e.g. offered by the Center for Orbit Determination in Europe (CODE) [1].

2.2. Dynamical model

For given models of the acceleration as a function of time t, position $\boldsymbol{r}$, and velocity $\boldsymbol{v}$, the motion of a satellite can be obtained from given initial conditions using a step-wise numerical integration. Without loss of generality we employ a first-order differential equation of motion for the six-dimensional state vector $\boldsymbol{y} = (\boldsymbol{r}; \boldsymbol{v})$, which can be handled by common integration methods. The least-squares orbit determination module of GHOST uses the variable-order variable step-size multi-step method DE of Shampine and Gordon [24]. It has earlier been proven to be a highly efficient and flexible integrator for orbital dynamics problems with stringent accuracy requirements. However, the state vector updates performed in an extended Kalman filter design require a restart of the integrator at each measurement epoch and therefore render the use of a high-order integrator inefficient. A low-order single-step method is preferable under these conditions and the classical fourth-order Runge–Kutta method has proven to be well-suited for representative measurement intervals of 30 s.

The modeling of gravitational and non-gravitational forces within the GHOST software follows the general discussion in [19]. In all test cases described later a 100×100 subset of the GGM01S gravity model [27] was employed. Compared to the full 120×120 model, the truncated version offers a 20% reduction in the overall processing without degrading the achieved orbit determination accuracy. For drag computations a Jacchia 71 atmospheric density model [9,19] has been adopted as a compromise between modeling accuracy and computational effort. Further information on the employed dynamical model, parameter sets and reference system conventions are summarized in Table 1.

Table 1
Overview of dynamical models and reference system transformations employed in the GHOST suite for GRACE orbit determination

Item	Description	References
Static gravity field	GGM01S 100×100 (selectable)	[27]
Tides	Solid Earth tide (4×4, diurnal)	[16,26]
	Polar tide	
	Ocean tides UT/CSR 3.0 + TEG2B (selectable)	
Luni-solar gravity	Analytical series expansions of luni-solar coordinates	[19]
Radiation pressure	Solar radiation pressure (canon-ball model; conical Earth shadow)	[19]
Atmospheric drag	Jacchia 71 density model	[9,19,22]
	NOAA solar flux (daily) and geomagnetic activity (3 hourly)	
Antenna offset	Constant phase center coordinates in s/c body system	
	Attitude quaternions describing s/c orientation in EME2000 system	
Empirical accelerations	Piece-wise constant accelerations in radial, transverse, and normal direction	
Terrestrial reference frame	ITRF2000 (implied by IGS/CODE GPS ephemerides)	
Earth orientation	IAU1976 precession	[15]
	IAU1980 nutation	
	IAU1982 sidereal time	
	IERS polar motion	
	IERS UT1-GPS	
Inertial reference frame	EME2000 (implied by reference transformations)	

Partial derivatives of the spacecraft state vector with respect to the epoch state, the drag and solar radiation pressure as well as empirical accelerations are obtained from a numerical integration of the associated variational equations [19]. Compared to the equations of motion, some simplifications (2nd order gravity field, neglect of luni-solar and tidal perturbations) may, however, be applied in the variational equations to reduce the resulting computational effort.

2.3. Empirical accelerations

To compensate for any deficiencies in the employed dynamical model, piecewise constant empirical accelerations (a_R, a_T, a_N) in the radial, transverse (along-track) and normal (cross-track) direction

$$\mathbf{e}_R = \frac{\boldsymbol{r}}{|\boldsymbol{r}|}, \qquad \mathbf{e}_T = \mathbf{e}_N \times \mathbf{e}_R, \qquad \mathbf{e}_N = \frac{\boldsymbol{r} \times \boldsymbol{v}}{|\boldsymbol{r} \times \boldsymbol{v}|} \tag{1}$$

are considered. The amplitude of these acceleration components is not known beforehand but estimated as part of the orbit determination process.

Following Bierman [4], the theory of random processes with exponentially correlated (or "colored") process noise provides a suitable mathematical framework for the description of unmodeled accelerations. A first-order Gauss–Markov process $p(t)$ [3] exhibits an exponential autocorrelation

$$R(\Delta t) = E\big(p(t), p(t+\Delta t)\big) = \sigma^2 \mathrm{e}^{-|\Delta t|/\tau}, \tag{2}$$

where σ^2 denotes the steady-state variance of the process and τ is the correlation time scale. In a time-discrete form, the process satisfies the first-order difference equation

$$p(t_{i+1}) = m_i \cdot p(t_i) + w_i \tag{3}$$

with mapping factor

$$m_i = \mathrm{e}^{-|t_{i+1}-t_i|/\tau}, \tag{4}$$

in which the process noise w_i is an uncorrelated random sequence with zero mean and variance

$$E(w_i^2) = \sigma^2(1 - m_i^2). \tag{5}$$

For practical purposes, the empirical accelerations are considered to be piecewise constant in pre-defined sub-intervals, which facilitates both the trajectory propagation and the overall parameter adjustment. In case of a batch least-squares estimator, the entire data arc is divided into n_a intervals of equal duration Δt and an independent set of empirical acceleration parameters $(a_R, a_T, a_N)_j$ is estimated for each interval $j = 0, \ldots, n_a - 1$. A priori information is used in the normal equations to constrain the individual parameters to a nominal value of zero with a predefined weight. The choice of an adequate interval length reflects a compromise between observability, computational effort and the capability to resolve time varying phenomena. Given an orbital period of roughly 6000 s for LEO satellites and a representative measurement interval of 30 s, intervals of 600 s duration have been found to be most suitable and adopted throughout this study. While shorter intervals provide a smoother variation of the estimated accelerations, no relevant improvement of the overall orbit determination accuracy has been observed that would justify the associated increase in computation time. Longer intervals, in contrast, appeared insufficient to sample the characteristic time scales of the empirical acceleration variation.

In the Kalman filtering approach, the estimation state vector is augmented by a three-dimensional empirical accelerations vector and an updated parameter set $(a_R, a_T, a_N)_i$ is obtained at each measurement epoch t_i. In between measurements, the empirical accelerations are assumed to be constant and the latest estimate is used in the dynamical trajectory propagation.

2.4. Least-squares orbit determination

The least-squares (LSQ) orbit determination process comprises the iterative adjustment of dynamical trajectory parameters and measurement model parameters from a given set of observations. Starting from given a priori conditions, the spacecraft trajectory is numerically integrated across the entire data arc and residuals are obtained as the difference between observations and modeled measurements. Making use of the partial derivatives with respect to the parameters of interest, corrections to the a priori parameters can then be obtained from the least-squares solution of an over-determined linear set of equations. Multiple iterations are required to cope with the non-linearity of the estimation problem, and convergence is typically achieved within a few (1–4) iterations.

With the above considerations, the estimation parameter vector comprises the following set of unknowns: the 6-dimensional spacecraft state vector $\boldsymbol{y}_0 = \boldsymbol{y}(t_0)$ at a reference epoch t_0, a solar radiation pressure coefficient C_R that acts as an adjustable scaling factor for the surface reflectivity in the modeling of solar radiation pressure forces, a drag coefficient C_D that acts as an adjustable scaling factor in the modeling of drag forces, empirical accelerations $\boldsymbol{a}_j = (a_R, a_T, a_N)_j$ in consecutive time intervals $[t_0 + j \cdot \Delta t, t_0 + (j+1) \cdot \Delta t]$, receiver clock offsets $c\delta t_i$ at each measurement epoch t_i $(i = 0, \ldots, n_T - 1)$, a carrier-phase or GRAPHIC bias B_k for each arc ("pass") of continuous carrier-phase tracking of a single GPS satellite.

For ease of notation, the individual estimation parameters are subsequently grouped into the n_T-dimensional clock offsets vector

$$\boldsymbol{T} = (c\delta t_0; \ldots; c\delta t_{n_T-1}), \tag{6}$$

the dynamical estimation parameter vector

$$\boldsymbol{Y} = (\boldsymbol{y}; C_R; C_D; \boldsymbol{a}_0; \ldots; \boldsymbol{a}_{n_a-1}) \tag{7}$$

of dimension $n_Y = 8 + 3 \cdot n_a$ and the n_B-dimensional bias parameter vector

$$\boldsymbol{B} = (B_0; \ldots; B_{n_B-1}). \tag{8}$$

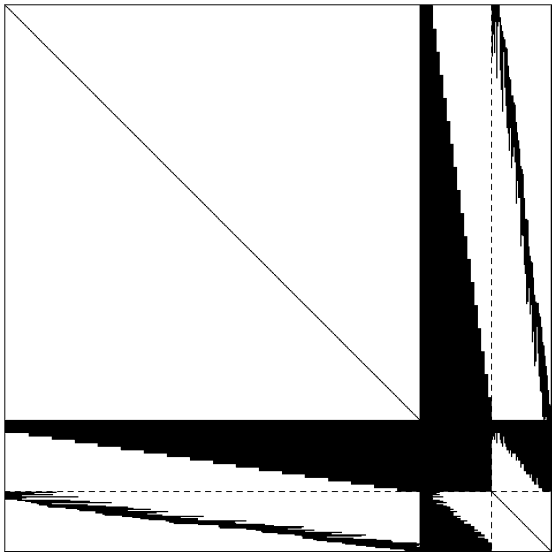

Fig. 1. Structure of normal equations for least-squares estimation of epoch-wise clock offsets, empirical accelerations and pass-by-pass carrier-phase biases.

A total of $n_T = 2880$ clock offsets need to be adjusted, for a one day data arc and a 30 s measurement interval, which notably exceeds the corresponding number of dynamical parameters ($n_Y = 440$ for 600 s empirical acceleration intervals) and bias parameters ($n_B \approx 400 \ldots 500$ for representative receivers and tracking conditions).

However, the construction and solution of the least-squares problem is greatly simplified by the specific structure of the associated normal equations

$$\left(\frac{\partial \boldsymbol{h}}{\partial(\boldsymbol{T},\boldsymbol{Y},\boldsymbol{B})}\right)^{\mathrm{T}} \boldsymbol{W}\left(\frac{\partial \boldsymbol{h}}{\partial(\boldsymbol{T},\boldsymbol{Y},\boldsymbol{B})}\right)\cdot\begin{pmatrix}\Delta\boldsymbol{T}\\ \Delta\boldsymbol{Y}\\ \Delta\boldsymbol{B}\end{pmatrix} = \left(\frac{\partial \boldsymbol{h}}{\partial(\boldsymbol{T},\boldsymbol{Y},\boldsymbol{B})}\right)^{\mathrm{T}} \boldsymbol{W}\big(\boldsymbol{z}-\boldsymbol{h}(\boldsymbol{T},\boldsymbol{Y},\boldsymbol{B})\big). \tag{9}$$

These are used to compute corrections $(\Delta\boldsymbol{T};\Delta\boldsymbol{Y};\Delta\boldsymbol{B})$ of a priori parameter values from the vector of modeled observations $\boldsymbol{h}(\boldsymbol{T},\boldsymbol{Y},\boldsymbol{B})$, the vector of measurements $\boldsymbol{z}$ and the inverse measurement covariance $\boldsymbol{W}$. As illustrated in Fig. 1, the normal equations matrix is not fully populated and sparse matrix techniques can be applied in storing and handling the individual matrix elements. Using the short form notation

$$\begin{pmatrix}\boldsymbol{N}_{TT} & \boldsymbol{N}_{TY} & \boldsymbol{N}_{TB}\\ \boldsymbol{N}_{YT} & \boldsymbol{N}_{YY} & \boldsymbol{N}_{YB}\\ \boldsymbol{N}_{BT} & \boldsymbol{N}_{BY} & \boldsymbol{N}_{BB}\end{pmatrix}\begin{pmatrix}\Delta\boldsymbol{T}\\ \Delta\boldsymbol{Y}\\ \Delta\boldsymbol{B}\end{pmatrix} = \begin{pmatrix}\boldsymbol{n}_T\\ \boldsymbol{n}_Y\\ \boldsymbol{n}_B\end{pmatrix} \tag{10}$$

of the normal equations, it may be recognized that only $\boldsymbol{N}_{YY}$ is a full matrix. In contrast to the dynamical parameters $\boldsymbol{Y}$ the partials with respect to $\boldsymbol{T}$ and $\boldsymbol{B}$ result in a large number of zero elements and sparsely filled matrix blocks. $\boldsymbol{N}_{TT}$, in particular, is a pure diagonal matrix, since measurements depend on only one clock offset parameter at each epoch. Likewise $\boldsymbol{N}_{TB}$ and its transpose exhibit a narrow band structure (assuming a proper ordering of the bias parameters), since measurements at a specific epoch depend only on a limited number of bias parameters. More specifically, the number of non-zero elements in each row of $\boldsymbol{N}_{TB}$ (or column of $\boldsymbol{N}_{BT}$) is always limited by the number of active tracking channels. $\boldsymbol{N}_{TY}$ and its transpose, finally, exhibit a triangular structure which reflects the fact that the number of empirical acceleration parameters, on which the measurements at a particular epoch depend, increases continuously towards the end of the data arc.

To solve the normal equations, the dynamical and bias parameters are combined into a common vector $\boldsymbol{X} = (\boldsymbol{Y},\boldsymbol{B})$. The unknown clock offset parameters are now eliminated using the formal solution

$$\Delta\boldsymbol{T} = \boldsymbol{N}_{TT}^{-1}(\boldsymbol{n}_T - \boldsymbol{N}_{TX}\Delta\boldsymbol{X}), \tag{11}$$

which results in the reduced equation

$$\Delta\boldsymbol{X} = (\boldsymbol{N}_{XX} - \boldsymbol{N}_{XT}\boldsymbol{N}_{TT}^{-1}\boldsymbol{N}_{TX})^{-1} \times (\boldsymbol{n}_X - \boldsymbol{N}_{XT}\boldsymbol{N}_{TT}^{-1}\boldsymbol{n}_T) \tag{12}$$

for the corrections of the dynamical and bias parameters. Compared to a direct solution of the full normal equations, the reduced system exhibits a notably lower operations count and can be solved in adequate times even for a large number of measurement epochs n_T. The clock parameter correction vector $\Delta\boldsymbol{T}$ may finally be obtained by re-substituting $\Delta\boldsymbol{X}$ into Eq. (11).

To constrain the solution and avoid potential singularities, statistical a priori information may be added to the normal equations as discussed in [19] and [18]. The use of a priori information is even mandatory, when no pseudo-range observations are processed along with carrier-phase or GRAPHIC data. Otherwise, a common change in all biases could not be distinguished from a shift of all clock offsets, thus yielding a rank deficit normal matrix. Because the incorporation of a priori information leaves the fundamental structure of the normal equations unchanged, the block elimination technique can likewise be used for an efficient computation of the solution vector.

2.5. Extended Kalman filter/smoother

Kalman filtering offers an alternative technique for orbit determination, which is particularly useful for real-time applications in view of its recursive nature. Starting from given initial conditions at an epoch t_{i-1}, the estimation state vector $\boldsymbol{Y}_{i-1}^{+}$ and its covariance $\boldsymbol{P}_{i-1}^{+}$ are propagated to the epoch t_i of the next measurement as part of the time-update step. In the subsequent measurement-update step, information from the observations is merged into the propagated state $\boldsymbol{Y}_i^{-}$ with a weighting factor (Kalman gain) that depends on the measurement accuracy and the propagated covariance $\boldsymbol{P}_i^{-}$. The post measurement-update values $\boldsymbol{Y}_i^{+}$ and $\boldsymbol{P}_i^{+}$ are then propagated to the subsequent epoch and the scheme is repeated as long as new observations become available. Since the fundamental concept of Extended Kalman Filters (EKF) for spacecraft navigation is well discussed in the literature (see

e.g. [19]) the following discussion focuses on those aspects that are of prime relevance for GPS-based precise orbit determination.

In analogy with the least-squares estimation, the Kalman filter state

$$\boldsymbol{Y} = (\boldsymbol{r}; \boldsymbol{v}; C_\mathrm{R}; C_\mathrm{D}; \boldsymbol{a}; c\delta t; \boldsymbol{b}) \tag{13}$$

in the present study comprises the spacecraft position and velocity vector $(\boldsymbol{r}, \boldsymbol{v})$ in the inertial reference frame (EME2000, ITRF), the radiation pressure and drag coefficients $(C_\mathrm{R}, C_\mathrm{D})$, empirical acceleration vector $\boldsymbol{a} = (a_\mathrm{R}, a_\mathrm{T}, a_\mathrm{N})$ in radial, tangential and normal direction as well as the clock offset parameter $c\delta t$ and carrier-phase (or GRAPHIC) bias parameters $\boldsymbol{b} = (B_0, \ldots, B_{n-1})$ for all simultaneously tracked GPS satellites. Considering, for example, a twelve channel receiver, the estimation state vector thus contains a maximum of 24 elements.

In between two measurement epochs, the position/velocity vector is propagated by numerical integration of the equations of motion using the rigorous dynamical model discussed earlier. Furthermore, simplified variational equations are numerically integrated to obtain the state transition matrix for the position/velocity vector and the partials with respect to the dynamical parameters $(C_\mathrm{R}; C_\mathrm{D}; \boldsymbol{a})_{i-1}$. A simple, fourth-order Runge–Kutta integration method is employed in both cases, which is most suitable for typical measurement intervals of 10–30 s.

Within the trajectory integration, the empirical accelerations $\boldsymbol{a}$ are assumed to be piecewise constant between the measurement epochs, but propagated values

$$\boldsymbol{a}_i^- = \mathrm{e}^{-|t_i - t_{i-1}|/\tau} \boldsymbol{a}_{i-1}^+ \tag{14}$$

are determined in accord with the Gauss–Markov process model upon completing the time-update step. All other filter states remain unchanged between updates, i.e.

$$(C_\mathrm{R}; C_\mathrm{D}; c\delta t; \boldsymbol{b})_i^- = (C_\mathrm{R}; C_\mathrm{D}; c\delta t; \boldsymbol{b})_{i-1}^+, \tag{15}$$

which reflects a white process noise model. Making use of the resulting state transition matrix, the covariance of the estimation parameters is likewise propagated to the new epoch. Finally, process noise $\boldsymbol{Q}$ for the empirical accelerations and the clock offset parameter is added to the propagated covariance $\boldsymbol{P}$ in proportion to the time interval between measurements (cf. (3)).

The subsequent measurement-update is formulated as a vector update involving all valid pseudo-range and carrier-phase observations collected at the same epoch. As in the case of the time-update, the basic Kalman filter equations proved to be adequate and no need for numerically more stable filter formulations like UD factorization, square root factorization or the Joseph algorithm (cf. [19]) was encountered in the practical applications.

To improve the accuracy of the Kalman filter solution, the entire data set is processed both in a forward direction and a backward direction. At each epoch, a smoothed solution

$$\overline{\boldsymbol{Y}} = \frac{\boldsymbol{P}_\mathrm{fwd}^{-1}\boldsymbol{Y}_\mathrm{fwd} + \boldsymbol{P}_\mathrm{bck}^{-1}\boldsymbol{Y}_\mathrm{bck}}{\boldsymbol{P}_\mathrm{fwd}^{-1} + \boldsymbol{P}_\mathrm{bck}^{-1}} \tag{16}$$

is then computed as the weighted average of the estimated state vectors from both runs [3,7]. The weights are determined by the information matrix (i.e. the inverse covariance) of the respective state estimates. By combining the forward and backward results, measurements from both before and after a given epoch contribute to the corresponding state estimate. As a result, a factor-of-two improvement in accuracy over the individual solutions can usually be achieved. However, a small degradation of the smoothed solution can be observed near the beginning and end of the data arc as well as extended data gaps, where either the forward or backward filter is not yet fully converged.

2.6. Data editing

The result of GPS-based precise orbit determination depends crucially on the proper screening of outliers and bad measurements that are even encountered in geodetic grade space receivers [20]. Within GHOST, GPS measurements are validated prior to the actual orbit determination process using a combination of different statistical tests and simple limit checks. User configurable thresholds are, for example, used to discard any observation below a certain elevation mask (e.g. 5°) or below a minimum signal-to-noise ratio (e.g. 20 dBHz for BlackJack GPS measurements). In addition, the quality of code and carrier-phase measurements is assessed in comparison with an a priori orbit. This a priori orbit is previously determined from a dynamical smoothing of pseudo-range-based single point navigation solutions using a high fidelity dynamical force model and adjusting empirical accelerations. Tests conducted with actual flight data have shown that the a priori orbit generated in this way has a representative accuracy of 1–2 m for single-frequency tracking and 0.25–0.5 m for dual-frequency tracking, which is fully adequate for data editing purposes.

At each epoch modeled ranges are computed using the a priori orbit and compared with the observed pseudo-ranges. From the set of $n \geqslant 2$ observations an estimate

$$c\delta t = \frac{1}{n}\sum_{k=1}^{n}\left(\rho_{\mathrm{PR},k} - \left(|\boldsymbol{r} - \boldsymbol{r}_{\mathrm{GPS},k}| - c\delta t_\mathrm{GPS}\right)\right) \tag{17}$$

of the clock bias at the measurement epoch and the associated residuals

$$\mathrm{res}_k = (\rho_{\mathrm{PR},k} - c\delta t) - \left(|\boldsymbol{r} - \boldsymbol{r}_{\mathrm{GPS},k}| - c\delta t_\mathrm{GPS}\right) \tag{18}$$

are obtained. Whenever the standard deviation of these residuals exceeds a predefined threshold, the observation which contributes the dominating error is identified and removed from the set of observations. If necessary, the process is repeated to reject multiple outliers at the same epoch. This

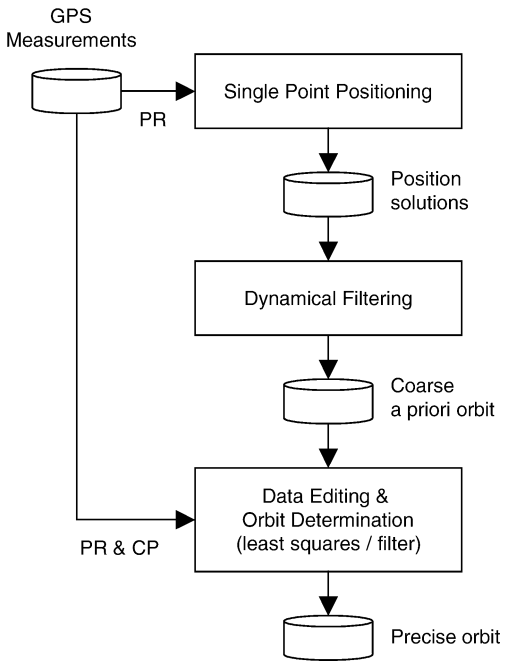

Fig. 2. Processing scheme for GPS based precise orbit determination of low-Earth orbiting satellites.

concept is likewise applicable for carrier-phase measurements (or GRAPHIC observations) when considering time differences between epochs. In this way, cycle slips or discontinuities in the carrier-phase tracking may safely be identified.

Practical tests with CHAMP and GRACE GPS measurements have clearly demonstrated the feasibility and robustness of this screening concept for both single- and dual-frequency data. Even though the generation of a coarse a priori orbit adds a notable burden to the overall orbit determination process, the approach was found to be more reliable and accurate than "on-the-fly" data screening within the least-squares adjustment or Kalman filtering. In any case, the resulting precise orbit determination concept (cf. Fig. 2) is fully self-contained and does not necessitate any external reference trajectory for initialization.

3. Results

The orbit determination techniques described above have been tested using actual flight data from the GRACE (Gravity Recovery and Climate Experiment) mission and validated using reference trajectories provided by the Jet Propulsion Laboratory (JPL) and the Technical University of Munich (TUM).

3.1. GRACE mission and GPS data

GRACE is a joint US–German science mission for accurate determination of the Earth gravity field and its temporal variation. It comprises two identical spacecraft flying at a separation of nominally 220 km in a near-polar orbit of roughly 450 km altitude. Both spacecraft are equipped with an Instrument Processing Unit (IPU) that is based on JPL's BlackJack receiver and configured to track up to 10 GPS satellites. In parallel, the IPUs process K-band radar measurements and star camera data. Compared to CHAMP, the GRACE GPS measurements are of even better quality with representative pseudo-range errors of down to 8 cm. In particular, multipath errors as caused on CHAMP by cross-talk between two different antenna strings [20] are absent, since no occultation measurements are presently performed by the receiver.

3.2. Selected data sets

Level 1B data [5] from the GRACE mission have recently been publicly released by JPL and UT/CSR as part of the Physical Oceanography Distributed Active Archive Center (PODAAC) [23]. Among others, these data include GPS measurements (re-aligned to integer 10 s of GPS time), spacecraft attitude quaternions and precise reference ephemerides. Precise GPS ephemerides and high-rate (30 s) clock data were obtained from CODE, a facility of the Astronomical Institute of the University of Berne [1].

For the present study, an 11-day data arc (day of year 295–305, 2003) has been selected. This period covers a prominent solar storm and thus provides a challenging test case for precise orbit determination. On day 300, in particular, the solar flux value $F_{10.7}$ rose from a typical level of 100 up to 298. As a consequence of the solar storm, an increased number of charged particles was emitted, which caused a geomagnetic peak activity on the days of year 303–304. Here, the associated 3-hourly K_p index increased from typical values of 3–5 up to 9. Although the results of the present study remain essentially unaffected by ionospheric perturbations, it is noted that the typical maximum total electron content (TEC) increased from 90 to 230 TEC units in that period. As a consequence, major degradations of the position accuracy would occur if the orbit determination solution were solely based on single-frequency pseudo-range data.

3.3. Dual-frequency orbit determination results

The results from least-squares orbit determination runs making use of ionosphere free dual-frequency code and carrier-phase measurements of the GRACE-B spacecraft are collated in Table 2. Here, typical position root-mean-square errors with respect to a JPL reference solution of about 4 cm are achieved. The along-track error with an average of 2.7 cm slightly exceeds the contributions from the normal component (2.4 cm) and the radial component (1.7 cm). This may be attributed to the fact that the employed reduced dynamic model imposes the strongest constraints in a direction perpendicular to the orbital motion. Kinematic GPS positions, in contrast exhibit the largest errors in the vertical

Table 2
GRACE-B least-squares orbit determination results using dual-frequency code and carrier-phase measurements. The columns provide the root-mean-square errors of the radial (R), along-track (T) and normal component (N) as well as the position (Pos) in comparison with the JPL reference solutions. In addition, a comparison with POD results of the Technical University of Munich (TUM) is provided

DOY	DLR-JPL			DLR-JPL	DLR-TUM	TUM-JPL
	R [cm]	T [cm]	N [cm]	Pos [cm]	Pos [cm]	Pos [cm]
295	1.6	3.1	2.7	4.4	7.1	7.6
296	1.5	2.3	2.2	3.5	4.7	3.9
297	2.0	2.6	2.3	4.0	5.7	5.0
298	1.5	2.7	2.4	3.9	5.6	4.8
299	1.6	2.9	2.4	4.1	6.3	4.5
300	2.0	2.6	2.1	3.9	6.9	5.3
301	1.9	2.6	2.5	4.1	5.5	4.6
302	2.9	3.3	3.0	5.3	7.2	6.3
303	5.3	7.7	2.6	9.7	15.6	13.2
304	2.9	4.4	2.6	5.9	8.2	8.0
305	2.1	3.0	1.9	4.2		
Mean 295–305	2.3	3.4	2.4	4.8	7.3	6.3
Mean 295–301	1.7	2.7	2.4	4.0	6.0	5.1

direction as a result of the asymmetric distribution of viewing directions (see e.g. [17,18]).

A common set of data weights, a priori variances and process noise values has been chosen for all days within the selected data arc and good orbit determination results are achieved both for "quite" days as well as days of high solar and geomagnetic activity. Worst case conditions are encountered on day 303 which exhibits a two hours data gap and covers a period of pronounced density variations. Even in this case the average orbit determination error stays below 10 cm when compared with the JPL orbit solution.

It must be noted, however, that the available GRACE reference orbits are themselves limited to an accuracy of several centimetres. This is obvious when comparing TUM and JPL reference orbits against each other which leads to typical position errors of 6 cm (3D rms). Similar results have been obtained in an assessment of GRACE orbit determination results performed by the Center for Space Research (CSR) at the University of Texas at Austin. Here, position errors of 5.8 cm (3D rms) where obtained when comparing CSR and JPL reference solutions [10]. As shown in Table 2, DLR and JPL orbits exhibit a somewhat better consistency (4 cm) than other sets of solutions.

For further reference, we note that slightly larger position errors (7–10 cm) have been obtained for the same data interval when processing data of the CHAMP satellite [8]. Aside from uncertainties in the employed reference orbits, the decreased performance in this case can be attributed to the less benign dynamical environment at the altitude of 390 km and the presence of multipath errors.

As illustrated in Fig. 3, the obtained orbits match the ionosphere-free code and carrier-phase measurements with a typical accuracy of 34 cm and 1.0 cm (standard deviation). In case of the pseudo-range residuals, this value reflects a P-code tracking noise of approximately 11 cm, which dominates other error sources. The carrier-phase residuals, in contrast, are governed by errors of the CODE 30 s-clock solutions for the GPS satellites and even larger residuals (3 cm) would be obtained when using IGS clock products at 5 min intervals. As shown by independent tests (see e.g. [20]) the actual carrier-phase noise is roughly one order of magnitude lower (1 mm) than the limitations implied by the GPS clock knowledge in an undifferenced processing scheme.

3.4. Single-frequency orbit determination results

Complementary to the previous section, the orbit determination accuracy achievable with single-frequency measurements has been assessed for the GRACE-B spacecraft. Making use of GRAPHIC observations formed from C/A code and carrier-phase measurements, a typical position accuracy of 7–8 cm has been achieved (Table 3). This is only slightly worse than in the dual-frequency case and reflects the excellent quality of the employed GPS receiver. The C/A-code noise amounts to less than 8 cm, which shows up in typical GRAPHIC residuals of 3.8 cm (Fig. 3). Even though this remarkable figure is, to some extent, specific to the BlackJack design, the results clearly demonstrate that single-frequency receivers with narrow correlator can well meet the precise orbit determination requirements of even advanced space missions.

3.5. Least-squares versus extended Kalman filter/smoother

Given the high communality between least-squares estimation and Kalman filtering, both methods can be expected to provide similar orbit determination results when employed with matching dynamical and measurement models. This is confirmed in Table 3, where single- and dual-frequency orbit determination results obtained with both methods are collated. Under typical dynamical conditions, the Kalman filter approach provides a position accuracy of 4.6 cm for dual-frequency and 6.9 cm for single-frequency measurements, which is only marginally worse than the least-squares estimator results discussed above.

However, the extended Kalman filter/smoother was found to be highly susceptible to extended data gaps, which is evident from the results obtained on day 303. Here, no GPS data are available for a 1.5 hours interval (21:10–22:50), during which the predicted state deviates notably (up to 8 m) from the reference orbit. Other than the least-squares estimator, the Kalman filter is unable to properly link measurements before and after the outage. As a consequence, the estimated empirical accelerations exhibit large errors in the transitional region, which are subsequently propagated throughout the data gap. While the impact of this problem can, to some extent, be reduced by tighter process noise settings, a modified tuning would reduce the filter's capability to compensate any deficiencies in the dynamical model.

Another potential disadvantage of the extended Kalman filter design results from the fact that the resulting trajec-

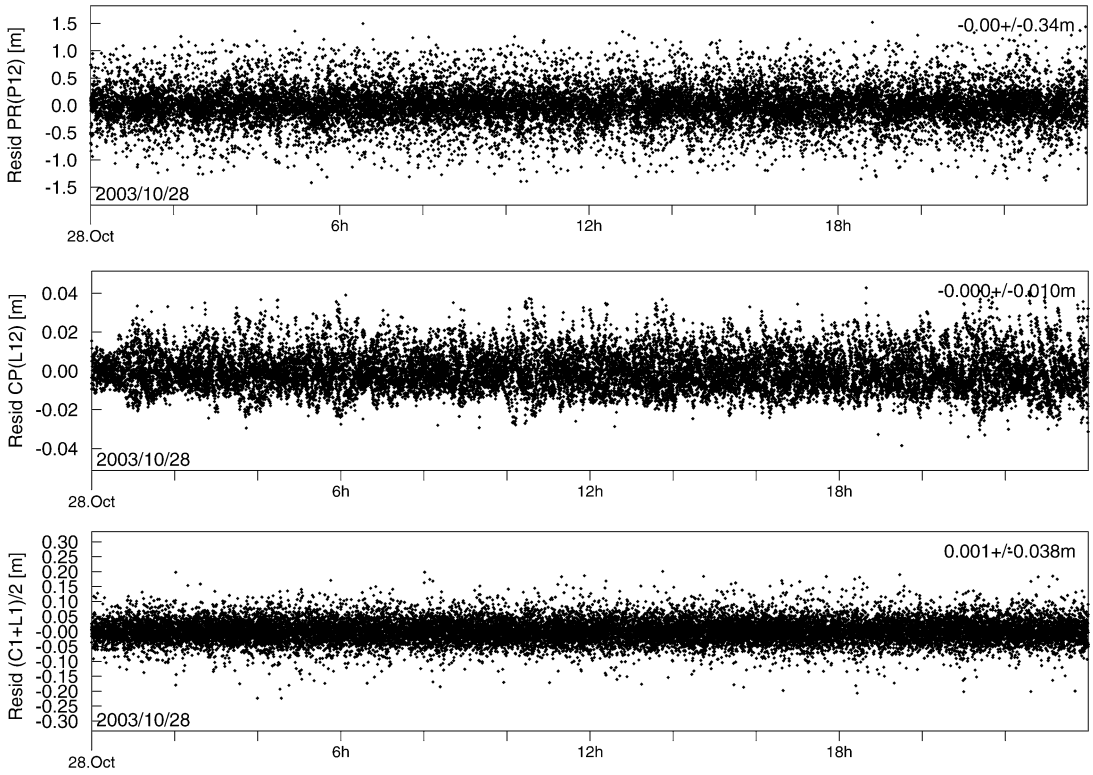

Fig. 3. Residuals of GRACE-B least squares orbit determination for 28 October 2003 (DOY 301): ionosphere-free pseudo-range residuals (top) and ionosphere-free carrier-phase (center) residuals from dual-frequency data processing; GRAPHIC residuals (bottom) from single-frequency processing.

Table 3
GRACE-B orbit determination results. Comparison of least-squares (LSQ) versus extended Kalman filter (EKF) solutions as well as single-frequency (1F) versus dual-frequency (2F) solutions. Root-mean square position errors are given with respect to the JPL reference trajectory

DOY	LSQ 2F [cm]	EKF 2F [cm]	LSQ 1F [cm]	EKF 1F [cm]
295	4.4	5.2	6.7	6.4
296	3.5	4.3	5.8	6.1
297	4.0	4.5	7.0	6.9
298	3.9	4.4	6.9	7.0
299	4.1	4.6	8.1	8.2
300	3.9	4.4	6.6	6.6
301	4.1	4.9	6.9	7.9
302	5.3	6.2	11.3	9.2
303	9.7	104.6	13.5	110.3
304	5.9	6.5	8.9	9.7
305	4.2	4.5	6.5	8.7
Mean 295–305	4.8	14.0	8.0	17.0
Mean 295–301	4.0	4.6	6.9	7.0

tory is not guaranteed to be smooth and differentiable. This is due to the fact that each measurement update causes a small discontinuity of the predicted state vector. The magnitude of this discontinuity depends on the data residuals (and thus the measurement and modeling accuracy) as well as the state covariance at the measurement epoch. A batch least-squares estimator, in contrast, always yields a set of initial conditions and dynamical parameters from which a continuous ephemeris is obtained. Here discontinuities are only present in the second derivative of the position vector due to the step-function approximation of the empirical accelerations. On the other hand, the long-arc integration performed within a least-squares orbit determination system are more likely to suffer from the accumulation of numerical errors than the short integration steps performed in a Kalman filter scheme. The practical impact of both effects and the merits of the different estimation schemes depends on the specifics of a particular software and the data set to be processed.

Regarding the overall system architecture, the extended Kalman filter/smoother based orbit determination software is notably less complex than its least-squares based counterpart. The number of estimation parameters is always restricted to 24 (for up to twelve simultaneously observed GPS satellites) and associated memory requirements are generally moderate. The least-squares approach, on the other hand, implies a large number of estimation parameters that grows near-linearly with the length of the processed data arc. Even worse, the storage requirements and the total operations count may grow with up to the second and third power of the arc length, respectively. This is also reflected in the higher computation times of the least-squares orbit determinations software employed in this study compared to a Kalman filter version (3.5 min versus 0.8 min for a 24 h data arc at 30 s steps on a 3 GHz Pentium PC).

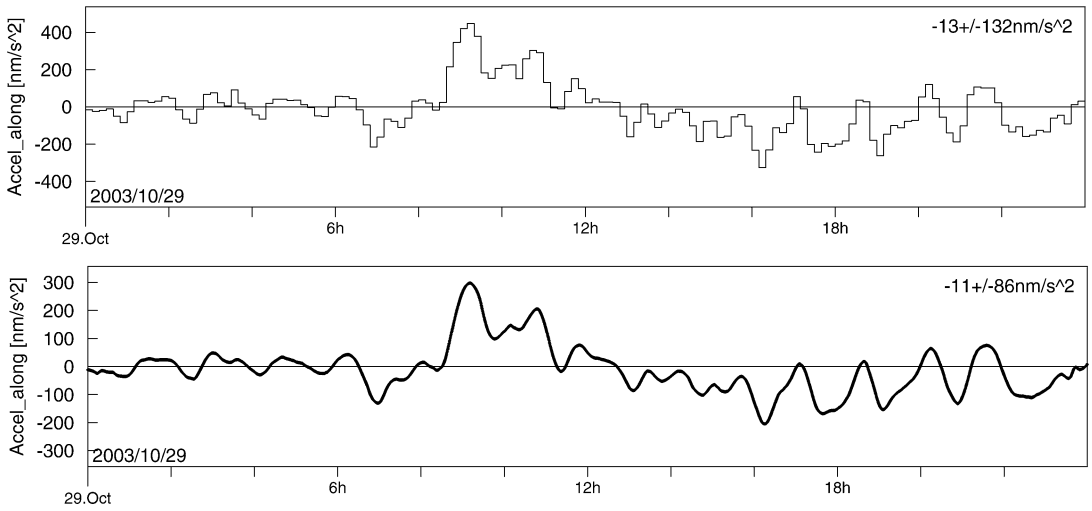

Fig. 4. Empirical accelerations of GRACE-B in along-track direction as estimated by the least-squares estimator (top) and Kalman filter (bottom) for 29 October 2003 (DOY 302).

3.6. Empirical accelerations

Typical results of the empirical accelerations estimated in orbit determination runs of least-squares and Kalman filter are depicted in Fig. 4. Here, only the dominant components in the tangential direction are shown. The normal components of the empirical accelerations are typically less than 20 $\mathrm{nm/s^2}$ and might be related to albedo, mis-modeled solar radiation pressure effects or unmodeled tidal perturbations. Since the tangential and the radial empirical acceleration components are difficult to separate, the estimates of the radial component have been constrained to near-zero by applying a tight a priori standard deviation and small process noise for this component.

The tangential components of the empirical acceleration in Fig. 4 show a small amplitude of 20 $\mathrm{nm/s^2}$ during the first hours of day 302, followed by a dramatic peak of 300 $\mathrm{nm/s^2}$ and a subsequent transition to a quasi-periodic behaviour. Over the total arc of 24 h, the standard deviation of the tangential component of the empirical acceleration is 86 $\mathrm{nm/s^2}$. The observed pattern of the tangential acceleration component mainly reflects a mismodeling of atmospheric drag in the applied dynamical model.

When comparing the empirical accelerations estimated by the least-squares and the Kalman filter scheme, it becomes obvious that the observed phenomena are highly correlated and consistent. However, it is noted, that the estimated amplitudes differ by a factor of about 1.5. The origin of this discrepancy has not yet been resolved but might be due to a coupling between empirical accelerations and other estimation parameters (e.g., C_R, C_D). It is further noted, that care must be taken when interpreting empirical acceleration patterns. The obtained values are not only highly dependent on the underlying dynamical models, but they are also dependent on the underlying stochastic models and the applied filter settings.

4. Summary and conclusions

Reduced dynamic orbit determination techniques have been analysed based on GPS data collected onboard the GRACE satellite in October 2004. It has been demonstrated that the use of a dual-frequency ionosphere-free combination of code and carrier measurements allows a precise reconstruction of the GRACE trajectory at a level of down to 4 cm (3D rms). When combining single-frequency narrow-correlator code and carrier measurements, a position accuracy of 7 cm (3D rms) has been achieved. The estimation of empirical accelerations as part of the orbit determination process enabled a highly accurate trajectory reconstruction even under the severe dynamic conditions of a massive solar storm in that period.

A similar orbit determination accuracy has been achieved both with a least-squares and an extended Kalman filter/smoother implementation. While the least-squares estimator treated the empirical accelerations as piecewise constant, the Kalman filter estimates were directly based on the assumption of a first-order Gauss–Markov process. The resulting empirical accelerations were found to be highly correlated between the two approaches. It has been shown that the strength of the extended Kalman filter/smoother lies in an efficient use of computer memory and processing time. The least-squares approach on the other hand, exhibits a better robustness and ensures smooth and differentiable trajectories. It must be emphasized though, that all results and conclusions are exclusively based on a comparison of algorithms described in the paper and implemented in the employed software. The consistent comparison of alternative concepts such as the pseudo-epoch state filter is left to further analysis.

The algorithms employed in the study account for the fact that Selective Availability has been deactivated and will not be present in future radio navigation signals. Based on

the available data set the feasibility of processing undifferenced GPS measurements in combination with IGS clock and ephemeris products has been demonstrated. This enables a lean software architecture and reduces the operational burden traditionally associated with GPS-based precise orbit determination.

Acknowledgements

The present study makes use of GPS measurements that have been made available by the GRACE project through the Center for Space Research, University of Texas at Austin, and the Jet Propulsion Laboratory, Pasadena. Furthermore, the authors would like to thank the anonymous reviewers for valuable comments and suggestions.

References

[1] AIUB, CODE 30 s clock solutions, ftp://ftp.unibe.ch/aiub/misc/products/HRRAPCLK, last accessed October 2004.
[2] S.B. Bisnath, R.B. Langley, Precise orbit determination of low Earth orbiters with GPS point positioning, in: ION National Technical Meeting, January 22–24, Long Beach CA, 2001, pp. 725–733.
[3] R.G. Brown, P.Y.C. Hwang, Introduction to Random Signals and Applied Kalman Filtering, third ed., Wiley, New York, 1997.
[4] G.J. Bierman, Factorization Methods for Discrete Sequential Estimation, Academic Press, New York, 1977.
[5] K. Case, G. Kruizinga, S. Wu, GRACE level 1B data product user handbook, JPL Publication D-22027, Jet Propulsion Laboratory, Pasadena, 2002.
[6] P. Fang, G. Gendt, T. Springer, T. Manucci, IGS near real-time products and their applications, GPS Solutions 4 (4) (2001) 2.
[7] D.C. Fraser, J.E. Potter, The optimum linear smoother as a combination of two optimum linear filters, IEEE Trans. Automat. Control AC-14 (4) (1969) 387–390.
[8] E. Gill, O. Montenbruck, Comparison of GPS-based orbit determination strategies, in: 18th International Symposium on Space Flight Dynamics, 11–15 October 2003, Munich, Germany, 2004, ESA SP-548.
[9] L.G. Jacchia, Revised static models of the thermosphere and exosphere with empirical temperature profiles, SAO Special Report 332, Cambridge, 1971.
[10] Z. Kang, P. Nagel, R. Pastor, Precise orbit determination for GRACE, Adv. Space Res. 31 (2003) 1875–1881.
[11] J. Kouba, P. Héroux, Precise point positioning using IGS orbit and clock products, GPS Solutions 5 (2) (2001) 12–28.
[12] D. Kuang, Y. Bar-Sever, W. Bertiger, S. Desai, B. Haines, T. Meehan, L. Romans, Precise orbit determination for CHAMP using GPS data from BlackJack receiver, in: ION National Technical Meeting, January 22–24, Long Beach, CA, 2001, Paper E1-5.
[13] R.B. Langley, O. Montenbruck, M. Markgraf, C.S. Kang, D. Kim, Qualification of a commercial dual-frequency GPS receiver for the e-POP platform onboard the Canadian CASSIOPE spacecraft, in: 2nd ESA Workshop on Satellite Navigation User Equipment Technologies, NAVITEC'2004, 8–10 December 2004, Noordwijk, The Netherlands, 2004.
[14] L. Marradi, E. Banfi, A. Mambretti, The Lagrange receiver: design and in-flight demonstration, NAVITECH'2001, 10–12 December 2001, Noordwijk (2001).
[15] D.D. McCarthy, IERS Conventions, 1996; IERS Technical Note 21, Central Bureau of IERS, Observatoire de Paris, Paris, 1996.
[16] D.D. McCarthy, G. Petit, IERS Conventions, 2003; Observatoire de Paris, Paris, 2003.
[17] P. Misra, P. Enge, Global Positioning System (GPS): Theory and Applications, Ganga-Jamuna Press, 2001.
[18] O. Montenbruck, Kinematic GPS positioning of LEO satellites using ionosphere-free single frequency measurements, Aerospace Science and Technology 7 (2003) 396–405.
[19] O. Montenbruck, E. Gill, Satellite Orbits, Springer-Verlag, Heidelberg, 2000.
[20] O. Montenbruck, R. Kroes, In-flight performance analysis for the CHAMP BlackJack GPS receiver, GPS Solutions (2003), submitted for publication.
[21] NASA, BlackJack GPS receiver, NASA Tech Briefs NPO-20891, 2001, http://www.nasatech.com/Briefs/June01/NPO20891.html.
[22] NOAA/SEC, Daily Space Weather Indices, US Dept. of Commerce, NOAA, Space Environment Center, 2003, ftp://ftp.sec.noaa.gov/pub/indices/dayind/, last accessed November 2003.
[23] PODAAC, Physical Oceanography Distributed Active Archive Center – Gravity Recovery and Climate Experiment, http://podaac.jpl.nasa.gov/grace/, last accessed October 2004.
[24] L.F. Shampine, M.K. Gordon, Computer Solution of Ordinary Differential Equations, Freeman, San Francisco, CA, 1975.
[25] P. Silvestrin, R. Bagge, M. Bonnedal, A. Carlström, J. Christensen, M. Hägg, T. Lindgren, F. Zangerl, Spaceborne GNSS radio occultation instrumentation for operational applications, in: ION-GPS-2000 Conference, Salt Lake City, 2000, pp. 872–880.
[26] UT/CSR, UTCSR Ocean Tide Model from Schwiderski and Interpolation/Extrapolation, Issue 10 September 2001, University of Texas, Center for Space Research, Austin, 2001, ftp://ftp.csr.utexas.edu/pub/grav/OTIDES.CSRC, last accessed October 2004.
[27] UT/CSR, GRACE Gravity Model GGM01, Center for Space Research, University of Texas, Austin, 2003, http://www.csr.utexas.edu/grace/gravity/ggm01/GGM01_Notes.pdf, last accessed October 2004.
[28] T. Van Helleputte, User manual for the GHOST orbit determination software, FDS-SUM-3110, Deutsches Zentrum für Luft- und Raumfahrt, Oberpfaffenhofen, 2004.
[29] S.C. Wu, T.P. Yunck, C.L. Thornton, Reduced-dynamic technique for precise orbit determination of low Earth satellites, J. Guidance Control Dynam. 14 (1) (1991) 24–30.
[30] T.P. Yunck, S.C. Wu, J.T. Wu, C.L. Thornton, Precise tracking of remote sensing satellites with the Global Positioning System, IEEE Transactions on Geoscience and Remote Sensing 28 (1) (1990) 108–116.
[31] T.P. Yunck, Orbit determination, in: B.W. Parkinson, J.J. Spilker (Eds.), Global Positioning System: Theory and Applications, AIAA Publications, Washington, DC, 1996.
[32] J.F. Zumberge, G. Gendt, The demise of selective availability and implications for the International GPS Service, Physics and Chemistry of the Earth (A) 26 (6–8) (2001) 637–644.